

PAPER • OPEN ACCESS

Automated Detection of Small-scale Magnetic Flux Ropes and Their Association with Shocks

To cite this article: Jinlei Zheng *et al* 2017 *J. Phys.: Conf. Ser.* **900** 012024

View the [article online](#) for updates and enhancements.

Related content

- [Observations and analysis of small-scale magnetic flux ropes in the solar wind](#)
Jinlei Zheng and Qiang Hu

- [Self-organization in magnetic flux ropes](#)
Vyacheslav S Lukin

- [Energetic Particles of keV–MeV Energies Observed near Reconnecting Current Sheets at 1au](#)
Olga V. Khabarova and Gary P. Zank

Automated Detection of Small-scale Magnetic Flux Ropes and Their Association with Shocks

Jinlei Zheng¹, Qiang Hu^{1,2}, Yu Chen¹, Jakobus le Roux^{1,2}

¹Department of Space Science, University of Alabama in Huntsville, USA

²Center for Space Plasma and Aeronomics Research, University of Alabama in Huntsville, USA

E-mail: jz0006@uah.edu, qh0001@uah.edu

Abstract. We have quantitatively examined one type of fundamental space plasma structures in the solar wind, the magnetic flux ropes, especially those of relatively small scales. They usually are of durations ranging from a few minutes to a few hours. The main objectives are to reveal the existence in terms of their occurrence and distributions in the solar wind, to quantitatively examine their configurations and properties, and to relate to other relevant processes, involving particle energization and intermittent structures in the solar wind. The technical approach is a combination of time-series analysis methods with the Grad-Shafranov reconstruction technique. This modeling method is capable of characterizing two and a half dimensional cross section of space plasma structures, based on in-situ spacecraft measurements along a single path across. We present the automated detection of flux ropes, construction of an online magnetic flux rope database, and detailed case studies of such structures identified downstream of interplanetary shocks.

1. Introduction

Small-scale magnetic flux ropes in the solar wind, i.e., those possessing the signatures of flux rope configuration from in-situ spacecraft measurements, were usually of relatively short durations, ranging from minutes to a few hours, compared with their large-scale counterparts, i.e., magnetic clouds (MCs) [1]. They were initially identified from the in-situ spacecraft measurements [2] at a much later time than the discovery of MCs. The same set of observations and analysis tools has been utilized in analyzing both sets of events. For example, these include the earlier identifying and categorizing effort of such events [3, 4], and associated modeling by the simple linear force-free cylindrical flux rope model. These events of durations \sim half an hour were also examined by more sophisticated Grad-Shafranov (GS) reconstruction technique in Hu and Sonnerup [5] which revealed the cylindrical helical field configuration of two small-scale flux rope events. Further detailed statistical analysis and associated analysis of additional observation signatures were carried out recently by Yu et al.[6]. However, up to date, the questions regarding their origination and their role in local particle energization remain.

Figure 1 (a) shows the rare observation of direct white-light imaging of solar atmosphere (corona) surrounding the solar disk during a total solar eclipse in 2008. The same observations but with much higher resolution are expected for the upcoming total solar eclipse over north America in August 2017. This black white picture reveals the plasma outflow as bright strands,



Content from this work may be used under the terms of the [Creative Commons Attribution 3.0 licence](#). Any further distribution of this work must maintain attribution to the author(s) and the title of the work, journal citation and DOI.

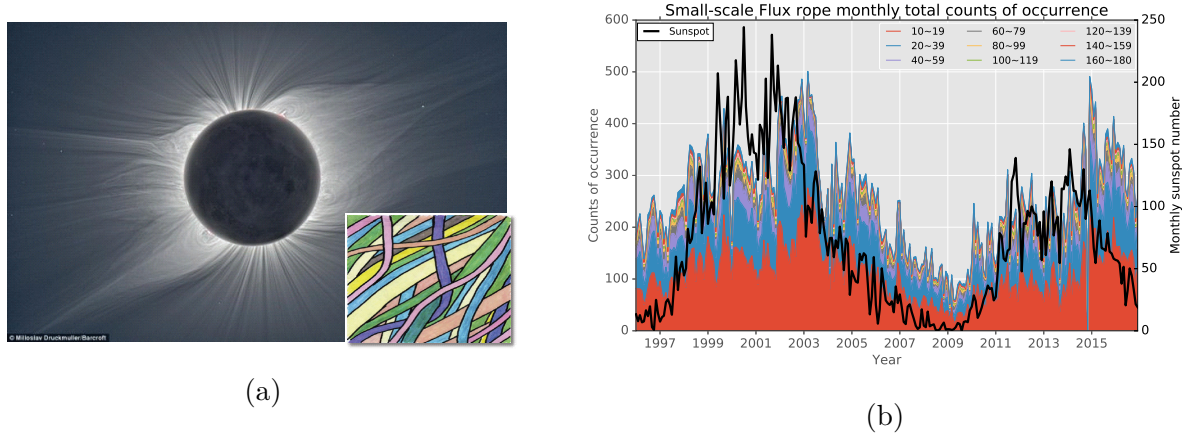


Figure 1. (a) The structured solar corona during a total eclipse. The bright streamline-like features represent plasma and magnetic structures. The inset depicts artistically one hypothetical scenario of “flux ropes” permeating the interplanetary space [7], originating from those filamentary structures near the Sun. (b) The monthly counts of flux rope events occurrence and the sunspot numbers (right axis) during 1996-2016.

channeled by the underlying magnetic field structures, otherwise invisible under normal conditions. It exhibits filamentary and fine-scale structures that constantly stretch outwards. At larger radial distances from the Sun, the outflows (i.e., solar wind) are further accelerated and become supersonic due to the interplay with the magnetic field. They carry along the embedded magnetic field structures and reach the distance of 1 AU at high but fairly constant speeds of hundreds of kilometers per second. A space probe, sitting in-between Sun and Earth, will sample these flows when they pass by, yielding time-series data equivalent to a set of spatial samples across the structure along a single path. The inset shows the artistic depiction of one hypothesis of the manifestation of such filamentary structures permeating the Sun-Earth space, where a spacecraft would cross such a “sea” of “spaghetti”-like strands. Each strand, or a tube in 3D is distinct from one another, as indicated by different colors, separated by well-defined boundaries. The internal structure of each tube can be characterized by a cylindrical flux rope configuration as to be demonstrated. So a spacecraft would cross multiple flux rope structures and associated boundaries along a single path at 1 AU.

Figure 1 (b) shows our preliminary result in identifying small-scale flux rope structures in the solar wind, with durations ranging from 10 to 180 minutes. We analyzed Wind spacecraft measurements from 1996 to 2016, covering nearly two solar cycles. We identified these small-scale structures via a novel approach to be described in the next section. Here we show the histogram of monthly event counts color-coded by event durations. The events of smaller durations generally have greater rates of occurrence. Clearly the total counts including all events of variable durations follow the monthly sunspot numbers, hinting at solar-cycle dependency of these events.

In contrast to their large-scale counterparts in the solar wind as direct consequences of energetic solar eruptions, these small to medium sized flux ropes are much less studied. The trend of their occurrence and properties varying with solar cycles as revealed from our preliminary analysis has yet to be firmly established. Lately, research interest in these structures and related processes has gained significant momentum [8, 9, 10, 11, 12, 13, 14, 15, 16, 17, 18]. It has been shown that these structures play critical roles in energizing suprathermal particles, an

important component of the particle population in the solar wind. They can also contribute to the presence of intermittent structures in the solar wind, an intrinsic ingredient in solar wind turbulence [19, 20, 21, 22, 23, 14, 24, 25]. Such intermittency, fundamental to the dynamic processes in solar wind plasmas, can be naturally explained by the presence of these flux rope structures, as depicted in Figure 1 (a), where the crossing of the flux ropes and their boundaries leads to discrete and abrupt changes in magnetic field and plasma properties, as manifested in time-series data. However such a hypothesis has yet to be verified. In addition, theoretical investigations [10, 26, 27, 28] envisaged the indispensable role of the existence of and interaction among these structures, responsible for trapping and energization of charged particles in space. Therefore it is of significant intellectual merit to quantitatively examine these structures, to elucidate their configuration and to establish their correspondence to closely related processes, from direct spacecraft measurements.

2. Small-scale Magnetic Flux Rope Database

To uncover the intuitive image of small-scale flux ropes in the solar wind, we decided to build a comprehensive database via extensively event searching. Until now, we have built a small-scale magnetic flux rope database based on the observational data from Wind spacecraft, and we will extend the spacecraft data coverage to include ACE and Ulysses data in near future. This database covers the time period from 1996 to 2016, including 63,460 flux rope records in total.

The distinct feature of the database is that it is based on unique Grad-Shafranov reconstruction technique. The Grad-Shafranov method is a true two-dimensional (2D) method that can derive a 2D cross section of magnetic and plasma configurations in space from 1D spacecraft data. It has been developed and applied for a number of years [5, 29, 30, 31, 32, 33, 34, 35, 36]. We adopt the quasi-static magnetic flux rope configuration described by the Grad-Shafranov equation, and developed an detecting algorithm to scan in-situ spacecraft observational data to look for flux rope structures. The data used in flux rope detecting process include time-series magnetic field vectors, plasma bulk properties such as flow velocity, plasma temperature and density, including electrons when available. To guarantee the quality of the flux rope database, we set a series of criteria to rule out the non-flux-rope structures which may survive in the flux rope searching process. For example, to exclude Alfvénic structures, we applied Walen test to each flux rope candidate, and removed the records with slopes below -0.3 or above 0.3. Since the average magnetic field magnitude in the solar wind is about 5 nT, we removed the records with average magnetic field less than 5 nT. In this paper, we put emphasis on the statistical results derived from the flux rope database, leaving the detailed elaboration on the flux rope detecting method to a separate paper.

Figure 2 (a) is flux rope duration histogram. The y-axis represents the monthly counts of flux ropes in logarithmic scale. This histogram hints at two slopes separated by the 60 minutes tick, which means the occurrence frequency of flux ropes exponentially decreases as the increase of duration, and the power indices are different between the flux ropes with durations less than 60 minutes and those longer than 60 minutes. Note that the histogram has an elevated tail distribution (160~180 minutes bin). This high tail does not follow the frequency distribution trend of the flux ropes with durations longer than 60 minutes. Because of the different axial orientation and moving speed of each flux rope, the flux rope duration cannot accurately reflect the flux rope scale size. If a spacecraft passes through the flux rope cross section with a trajectory perpendicular to flux rope axial direction, it will surely take less time than the situation in which the spacecraft obliquely passes through the flux rope at equal speed. To check the frequency distribution of flux rope scale sizes, we derive the the flux rope size from its duration, orientation,

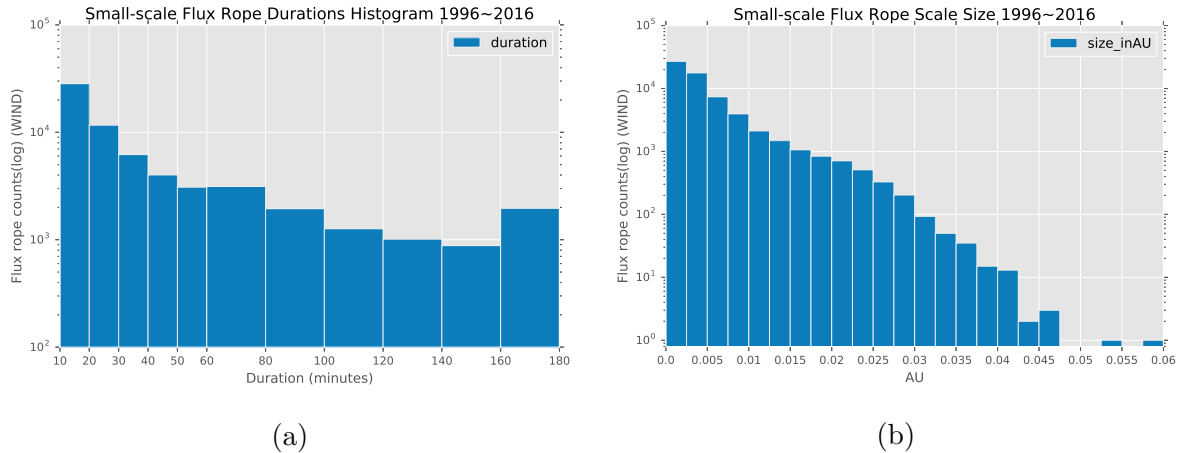


Figure 2. (a) Flux rope duration histogram. In flux rope detecting process, we split the entire task into 11 iterations with different window sizes. The window sizes are 10~20 minutes, 20~30 minutes, 30~40 minutes, 40~50 minutes, 50~60 minutes, 60~80 minutes, 80~100 minutes, 100~120 minutes, 120~140 minutes, 140~160 minutes, and 160~180 minutes. The bar plot represents the counts (log scale) of detected flux rope in each bin. (b) Flux rope scale size histogram. Derived from flux rope duration, orientation and the velocity of co-moving frame.

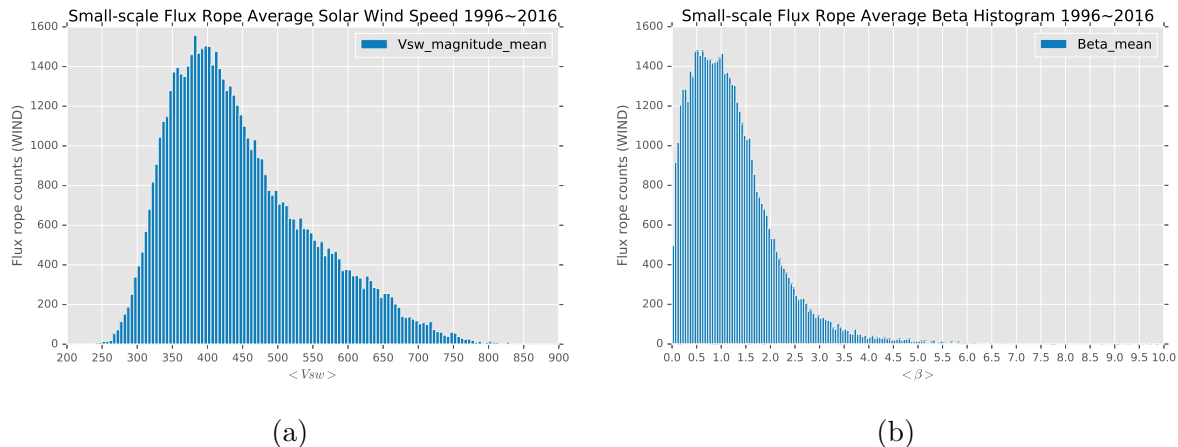


Figure 3. (a) Flux rope solar wind speed histogram. For each flux rope case, we calculated the average solar wind speed between the flux rope start and end time. (b) Flux rope plasma β histogram. The plasma β is calculated from proton and electron number density (assuming $N_e = N_p = N$), proton and electron temperature, and magnetic field. The electron temperature data has a gap from 2001/05/31 23:59:57 to 2002/08/16 00:00:05. The plasma β in this gap is not counted in the histogram.

and the co-moving frame velocity. Figure 2 (b) shows the flux rope scale size histogram. In this distribution, the relation between log(counts) and scale sizes seems to be bi-linear of similar slopes, with an “ankle”-like transition in between. There is no high tail as that in duration histogram. This indicates that effect on scale sizes by oblique passages is more pronounced for long-duration events. Figure 3 (a) is solar wind histogram corresponding to flux rope events. It indicates that the small scale flux ropes are more likely to occur in low-speed streams, with

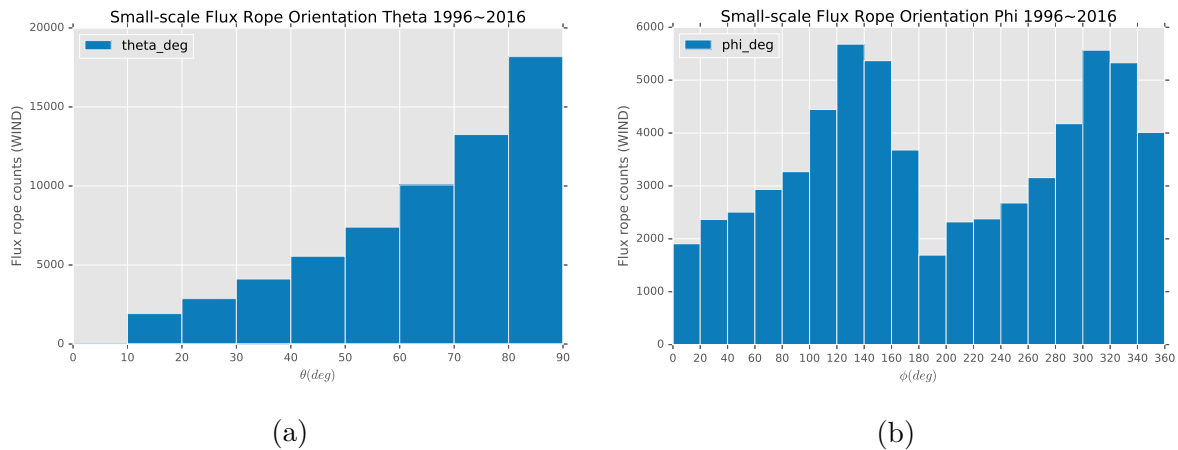


Figure 4. (a) Flux rope polar angle θ histogram. The actual polar angle range is from 0° to 180° . To cut down the time consuming in flux rope detecting process, we restrict end points of the direction vectors in upper hemisphere, and do not distinguish the vectors with opposite directions with each other. (b) Flux rope azimuthal angle ϕ histogram. This angle is the projection of flux rope axial directions onto ecliptic plane.

peak speed around 400 km/s. Figure 3 (b) is the histogram of average plasma beta within each flux rope interval. There is a clear and broad peak around value 1, indicating the significance of plasma pressure. Figure 4 (a) is the histogram of polar angle of flux rope axis, which implies that the projection of flux rope axis tend to lay between negative X-axis and Y-axis in GSE frame. Figure 4 (b) shows the histogram of azimuthal angle of the flux rope axis orientation in GSE coordinate. The unflat pattern implies a preference of small scale flux rope axis orientation is in the ecliptic plane.

3. Case Studies Associated with Shocks

Interplanetary shocks are known sources contributing to energetic particle acceleration and transport in the heliosphere. However evidences exist for certain energy-range particles to show behaviors departing from expected shock related acceleration processes. The association between structures (mainly discontinuities) other than shocks and local energetic particle flux enhancement was also reported by a number of studies [15, 21, 22, 9, 37]. Theoretical studies suggested that the combined diffusive shock acceleration and downstream multiple magnetic island acceleration would result in the energization of charged particles [27, 10]. We found in a previous study presented in the last year's conference [8] the existence of flux rope structure downstream of shocks and hinted at the correspondence to local particle energization. In the present study, we follow up with further analysis of the occurrence and properties of flux ropes downstream of shocks and the associated energetic particle signatures. In this section, we are going to present two sets of case studies in which the enhanced ions flux was observed within the flux rope region. We will use the combined observations of ACE and Wind spacecraft to illustrate the flux rope morphological change leading to energizing particles.

Our analysis employs existing online resources such as databases containing identified shock waves and other types of discontinuities or structures. For example, they include, but are not limited to, the online shock database from the ACE spacecraft at Earth, and the similar but more comprehensive Finnish Interplanetary Shock Database (<http://ipshocks.fi/>) that lists identified shock waves from multiple spacecraft in the solar wind. The associated shock parameters

such as the geometry of the shock, the shock speed, and compression ratios etc. are also given in these databases, which will be utilized by our analysis.

We checked the conditions near two interplanetary shocks. One shock was observed by ACE on March 10th, 1999, at 0:40 UT, and observed again by Wind after about 53 minutes. The other shock was observed by ACE on December 7th, 2003, at 13:41 UT, but not observed by Wind. We examine the magnetic field, solar wind plasma, and energetic ions data beginning from 1 hour upstream the shock and ending at 9 hours downstream the shock. In the 10 hours interval, a few flux ropes were detected, and the combined observations of ACE and Wind suggested the flux rope merging behavior in the region of enhanced energetic ion flux.

3.1. Case study: March 9th, 1999, 23:40 UT to March 10th, 1999, 09:40 UT

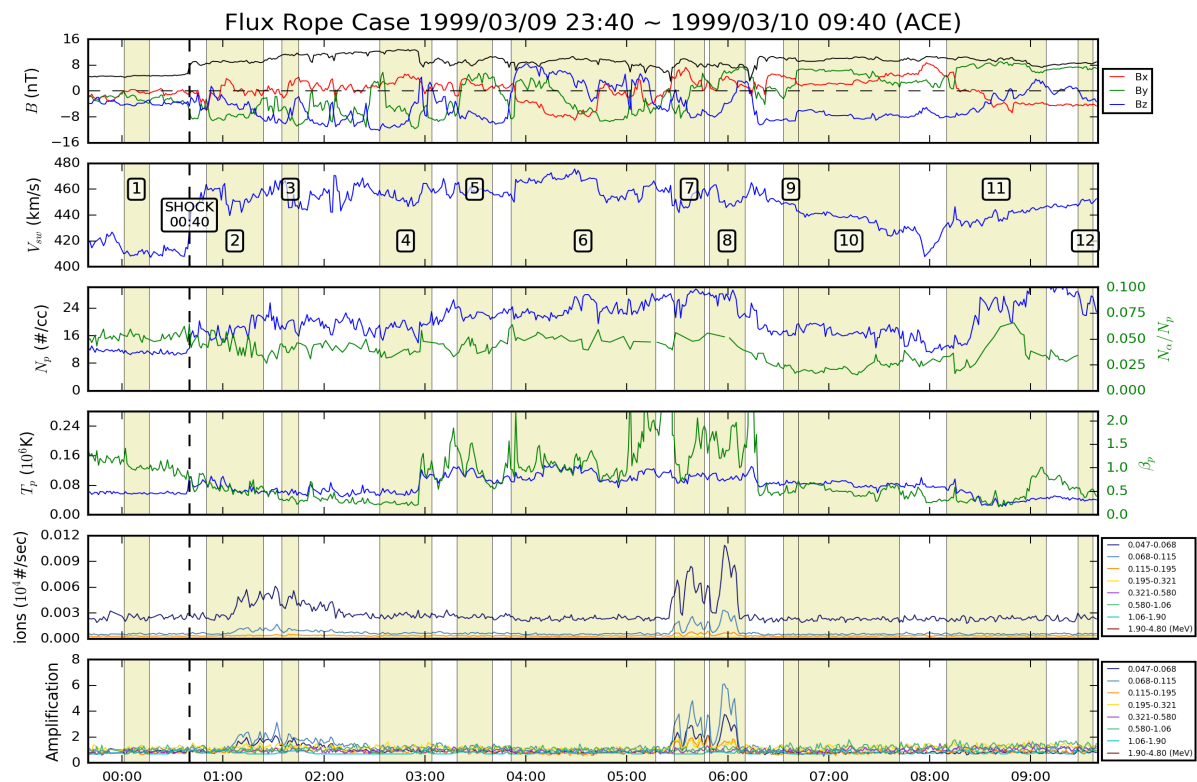


Figure 5. Time series data from March 9th, 1999, 23:40 UT to March 10th, 1999, 09:40 UT. All data are from ACE spacecraft. This time interval contains one interplanetary shock and twelve flux rope structures which are labeled from 1 to 12 and shaded by yellow color. The first panel is the magnetic field data. The black solid line denotes the total magnetic field magnitude. The second panel is the solar wind bulk speed. In the third panel, the proton number density is shown in blue and the alpha/proton ratio is shown in green. The fourth panel are the proton temperature (in blue line) and proton plasma beta (in green line). The fifth panel is ions flux, and the sixth panel is the same ions flux, but normalized by the value at shock time. The energy range of each curve is provided in the box to the right. The shock is denoted by a vertical black dashed line across six panels.

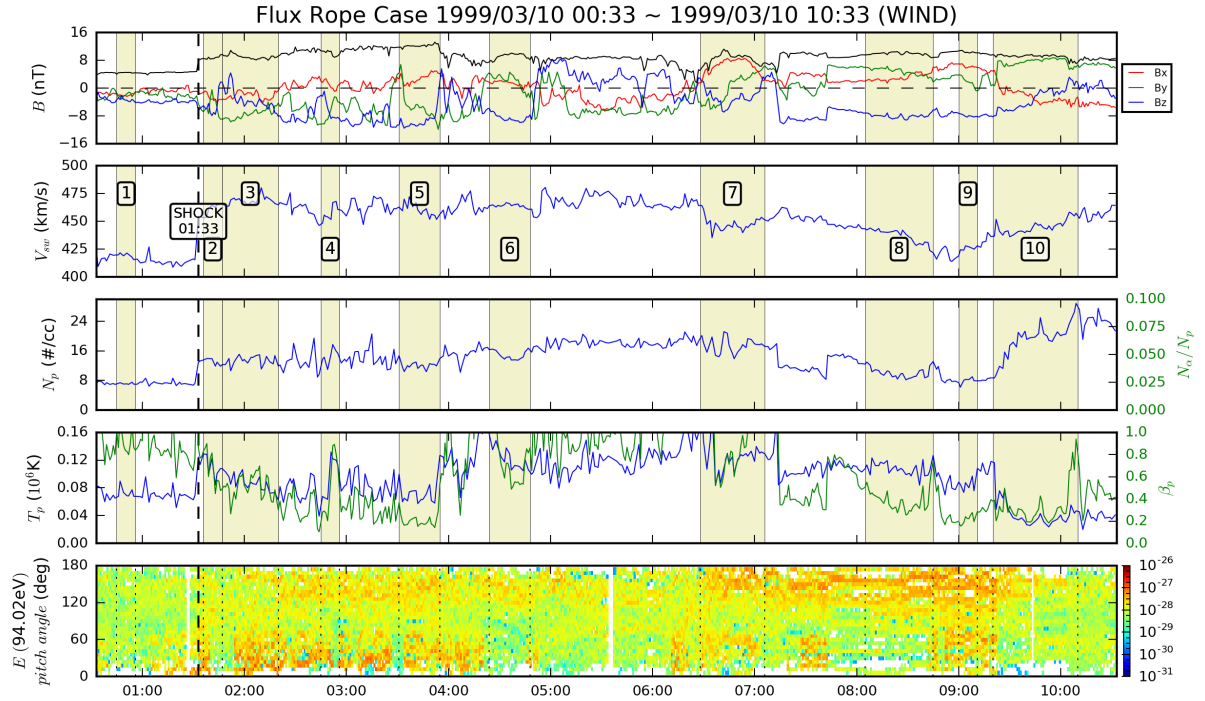


Figure 6. Time series data from March 10th, 1999, 00:33 UT to March 10th, 1999, 10:33 UT. All data are from Wind spacecraft. This time interval contains one interplanetary shock and ten flux rope structures which are labeled from 1 to 10 and shaded by yellow color. The first panel is the magnetic field data. The black solid line denotes the total magnetic field magnitude. The second panel is the solar wind bulk speed. In the third panel, the proton number density is shown in blue line and the alpha/proton ratio is shown in green line. The fourth panel shows the proton temperature (in blue line) and proton plasma beta (in green line). The fifth panel is suprathermal electron pitch angle distribution. The shock is denoted by a vertical black dashed line across five panels.

Figures 5 and 6 are time series data around the same shock observed by ACE and Wind successively. Figure 5 shows a shock observed at 00:40 UT, while in Figure 6, the shock time is 01:33 UT. The two observations have 53 minutes time shift. In Figure 5, we note that during the intervals of flux ropes No.7 and No.8, the ions flux is enhanced. Within the interval of flux rope No.7, the ions flux is enhanced by 5 times in 0.068 - 0.115 MeV channel and by 3 times in 0.047 - 0.068 MeV channel. In each case, the enhancement peak is near the center of the flux rope interval. Panels five and six show that after the shock time, there is a weak ion flux enhancement from 1:00 UT to 2:00 UT, and after 2:00 UT, the ions flux level is steady. Thereafter, starting at about 5:30 UT, the ion flux reaches two consecutive peaks. We believe that these two ion flux peaks are less likely caused by direct shock acceleration. Instead, they may be caused by other co-located processes, such as flux rope merging or contraction. Noting that these two flux ropes are next to each other, which makes the interacting with each other possible. If they are merging, we should be able to see one single flux rope after some time. In order to check their temporal evolution, we examined the flux rope events observed by Wind which are radially aligned with ACE at a distance of 247 Earth radii toward Earth. We found the correspondence to flux rope No.7 and No.8. In Figure 6, we can see that the Wind flux rope No. 7 has similar magnetic field structure to the combined intervals of ACE flux rope No.7 and No.8 in Figure 5.

1999-03-10 05:48 UT (ACE) 1999-03-10 05:50 UT (WIND)

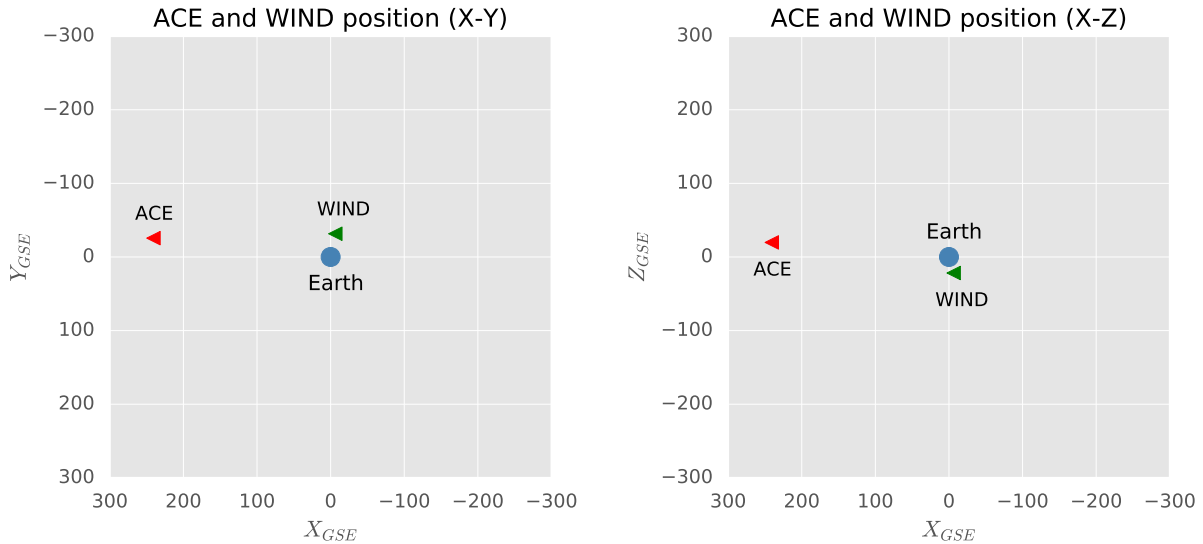


Figure 7. The positions of ACE and Wind spacecraft in GSE coordinate. The left panel is the projection on XY-plane, and the right panel is the projection on XZ-plane. The time stamp of ACE is March 10th, 1999, 5:48 UT, and the time stamp of Wind is March 10th, 1999, 5:50 UT. The unit of all axes is Earth radius.

Also, their surrounding magnetic field structures are highly similar. We believe the Wind flux rope No. 7 is the correspondence of ACE flux rope No.7 and No.8. To verify our speculation, we check the time shift of ACE and Wind flux ropes, and compare it with propagating time of solar wind. Figure 7 shows the positions of ACE (red triangle) spacecraft, Wind (green triangle) spacecraft, and the Earth (blue dot) in GSE coordinate when ACE is in the center of flux rope No.7 in Figure 5 (at about 5:48 UT). Since the flux rope propagating time is less than 2 hours, in such a short time, we can assume both spacecraft are stationary. We can see that the ACE and Wind are aligned along X_{GSE} axis, and ACE is in front of Wind in the direction toward the Sun. The GSE coordinate of ACE is $(X, Y, Z) = (1.53359 \times 10^6, -1.63047 \times 10^5, 1.25898 \times 10^5)$ km, and the GSE coordinate of Wind is $(X, Y, Z) = (-4.0486 \times 10^4, -2.0099 \times 10^5, -1.3872 \times 10^5)$ km. From their coordinates, we can calculate that the separation of ACE and Wind in X_{GSE} direction is 1.57408×10^6 km. From the second panels of Figure 5 and Figure 6, we can see that the average solar wind speed during the flux rope intervals under checking (No.7 and No.8 in Figure 5, and No.7 in Figure 6) is about 450 km/s. Therefore, the propagating time for a flux rope from ACE to Wind is about 58 minutes. Then we are going to check the time shift of flux rope No.7 and No.8 in Figure 5, and the flux rope No.7 in Figure 6. The center time of flux rope No.7 and No.8 in Figure 5 is 5:49 UT (the center between start time of flux rope No.7 and end time of flux rope No.8), while the center time of flux rope No.7 in Figure 6 is 6:47 UT. The time shift is 58 minutes, which is the same as the calculated propagating time. Now we are confident that the flux rope observed by Wind is the same ones but at later evolution phase of the flux rope No.7 and No.8 observed by ACE.

In order to show the flux rope evolution from ACE to Wind, we reconstructed the flux rope No.7 and No.8 in Figure 5, and the flux rope No.7 in Figure 6. Figure 8 (a) shows the recon-

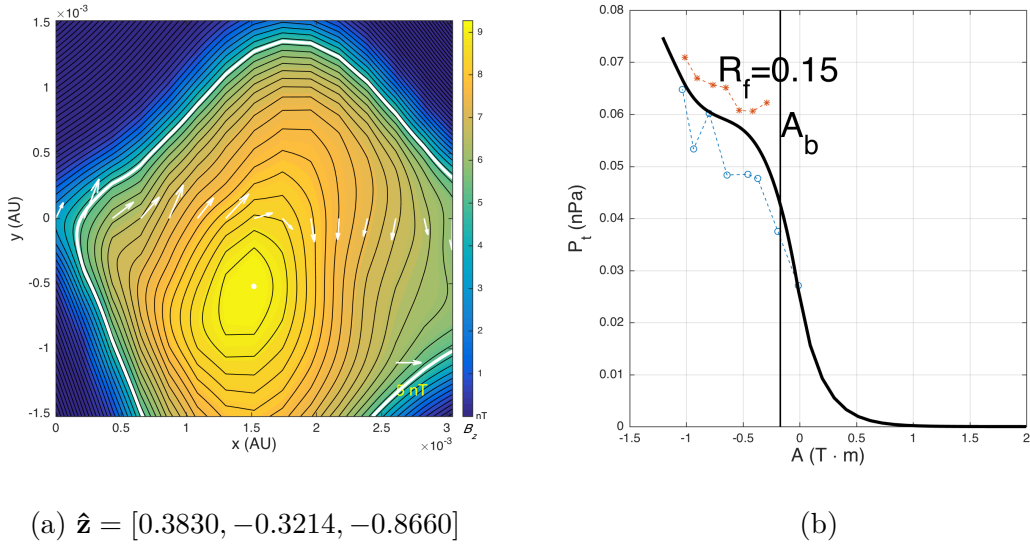


Figure 8. GS reconstruction result for flux rope record No.7 (March 9th, 1999, 05:28 - 05:46 UT) in Figure 5. (a) The cross-section magnetic field configuration of the flux rope. The unit vector $\hat{\mathbf{z}}$ represents the z axis orientation of the flux rope. The filled color contour represents the axial magnetic field B_z and the line contour overlapped in black represents the transverse magnetic field. The white arrows across the map horizontally are projected transverse magnetic field vectors along the spacecraft path. The white contour line encloses the region $A < A_b$ (or in some case, $A > A_b$), denoted in (b). The reconstruction map within this line is reconstructed by double-folded satellite data, and the region beyond this line is reconstructed based on the extrapolated data. (b) The fitting curve (bold solid line) of $P_t(A)$ for this flux rope case. The fitting is based on the data points denoted by blue circles and red stars, where the circles represent the data as satellite was crossing the first half of flux rope structure and the stars represent those of second half. The thin vertical solid line denoted by A_b marks the boundary corresponding to the white line in (a). A fitting residue R_f is denoted.

structured cross section of flux rope No.7 in Figure 5. The white arrows are the transverse field vectors along the projection of spacecraft trajectory on xy -plane. The color represents the B_z field of this flux rope. The arrow directions indicate that this flux rope has the left-handed chirality. The maximum B_z field is about 9 nT in the flux rope center. Figure 8 (b) is the fitting curve of $P_t(A)$, in which P_t is the transverse plasma pressure, the sum of plasma and axial magnetic pressure, and A is the magnetic vector potential. Though the fitting residue R_f is acceptable, the two branches of measured data points (in red and blue, respectively) still have notable deviations, which indicates that the current axial orientation we found may not be the optimal one. We will discuss it later when we analyze the axial orientation. Figure 9 (a) is the reconstructed cross section of flux rope No.8 in Figure 5, which is next to flux rope No.7. Its maximum B_z field is about 8.5 nT, which is relatively weaker than its neighbor. No.8 has the same left-handed chirality as No.7. Their $\hat{\mathbf{z}}$ axis orientations differ by 67° . Two neighboring flux ropes with the same chirality and interacting with an oblique angle between their cylindrical axes may merge due to magnetic reconnection [38].

Since No.7 and No.8 are close to each other, we tried to put these two flux rope together to see if we can find the combined structure. Figure 10 (a) is the reconstructed cross section when

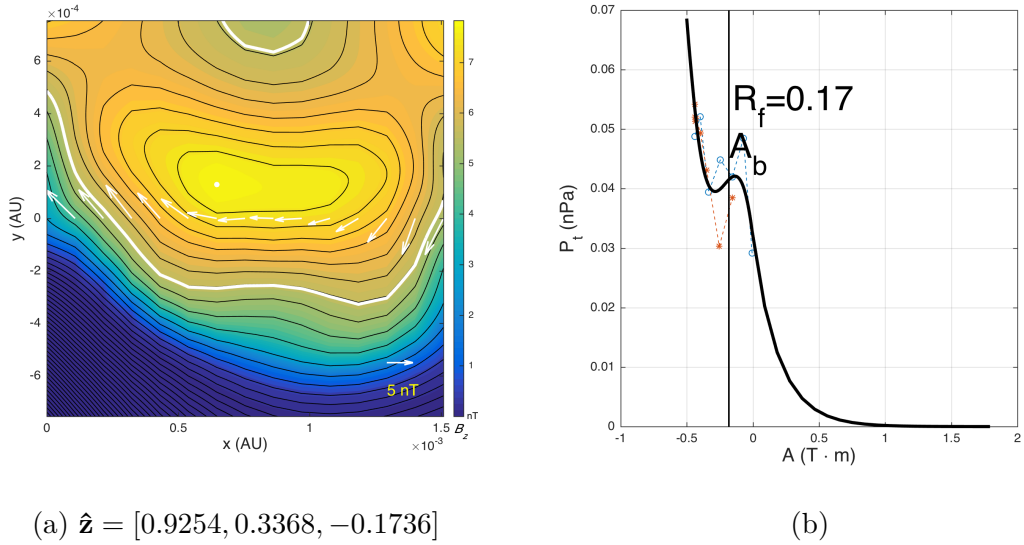


Figure 9. GS reconstruction result for flux rope record No.8 (March 9th, 1999, 05:49 - 06:10 UT) in Figure 5. The format is the same as Figure 8.

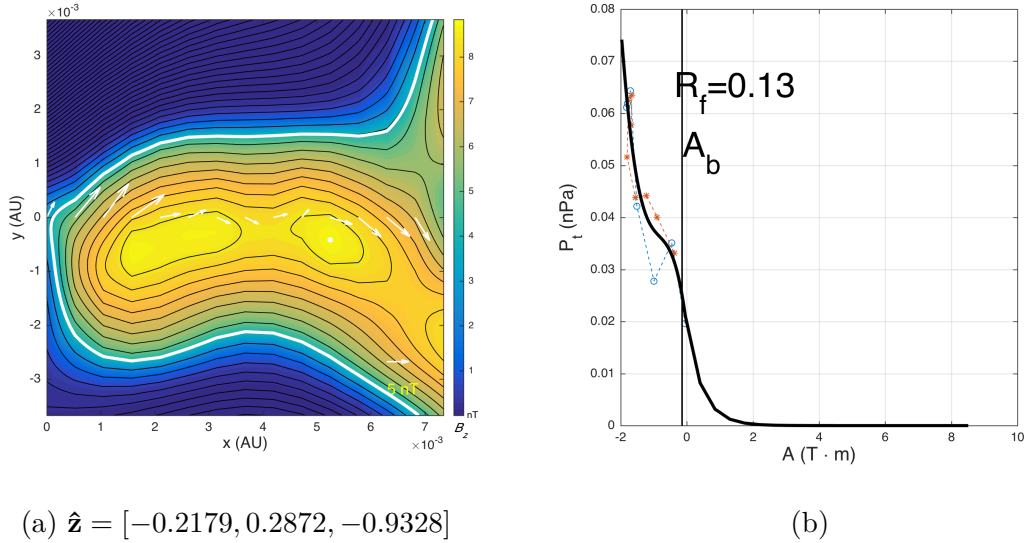


Figure 10. GS reconstruction result for the combination of flux rope No.7 and No.8 (March 9th, 1999, 05:28 - 06:10 UT) in Figure 5. The format is the same as Figure 8.

we put No.7 and No.8 together. A twin flux rope shape cross section is obtained. The fitting residue shown in Figure 10 (b) is smaller than both of the individual ones. When checking the axial orientation of each individual flux rope and comparing them with the combined flux rope, we found that they have three different axial orientations. This means the structures of flux rope No.7 and No.8 are not strictly 2-D structures. This is also partially the reason why the two individually reconstructed flux ropes do not have very small fitting residues.

Figure 11 (a) is the reconstructed cross section of flux rope No.7 in Figure 6. This flux

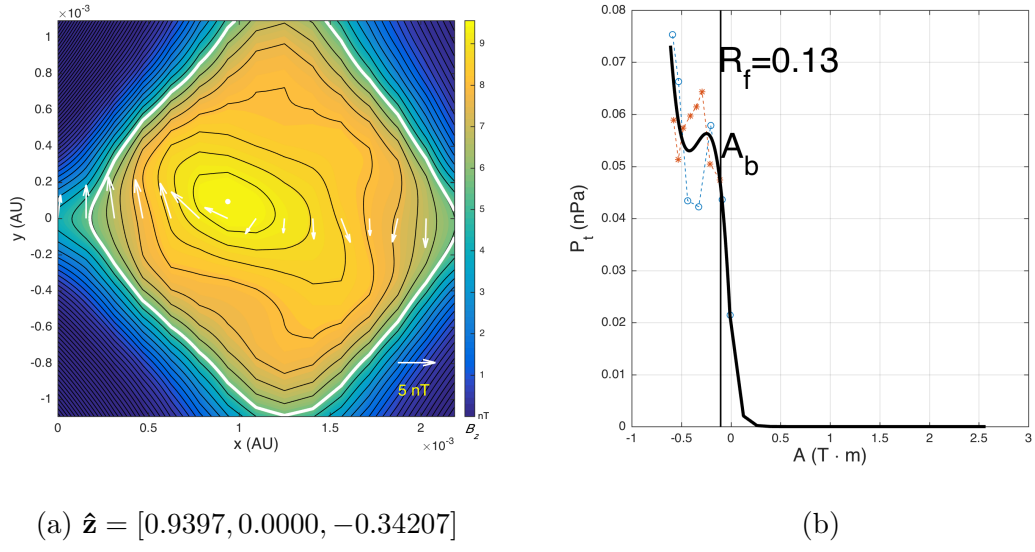


Figure 11. GS reconstruction result for flux rope record No.7 (March 9th, 1999, 05:49 - 06:10 UT) in Figure 6. The format is the same as Figure 8.

rope is observed by Wind and is the correspondence of the combined flux rope No.7 and No.8 observed by ACE in Figure 5. It has similar core field strength but smaller size compared with the combined flux rope observed by ACE. From Figure 10 (a) to Figure 11 (a), we see the twin flux rope structure merges into a single one. The irregular transverse field lines in Figure 11 (a) implies that this flux rope just underwent a non-steady evolution process. It is interesting to note that the axial orientation of the Wind flux rope is also different from the combined flux rope from ACE. The angle between their axial orientations is 83° . This shows that the flux rope orientation is subject to change in the merging or propagating process, either due to the overall rotation or the more complicated 3-D structures formed in merging process.

3.2. Case study: December 7th, 2003, 12:41 UT to 2003 December 7th, 22:41 UT

In this case study, another ions flux enhancement event during flux rope interval was observed, and the temporal evolution of the corresponding flux rope is analyzed. Figure 12 shows ACE time series data from December 7th, 2003, 12:41 UT to 22:41 UT. Figure 13 shows Wind time series data from December 7th, 2003, 12:00 UT to 21:00 UT. Figure 12 shows a shock observed at 13:41 UT, however, this shock was not observed by Wind in Figure 13. The 5th and 6th panels in Figure 12 show that there are two major flux rope enhancement events during the plotted time interval. The first event is right after the shock, and the other ions flux enhancement is from 15:29 UT to 16:41 UT, during which, a flux rope structure is detected and labeled as No.3. The first enhancement event is probably due to direct shock acceleration, while the second enhancement event may be caused by flux rope related acceleration [28, 27, 26]. Next, we will check the temporal evolution of flux rope No.3 in Figure 12. If this flux rope shows contracting feature when propagating, it could have the ability to boost the ions flux. In Figure 13, we found a possible correspondence to flux rope No.3 in Figure 12, whose time interval is from 17:17 to 18:08 and labeled as No.5. Same as the method we used in last case study, we are going to verify the correspondence by checking the ACE and Wind positions and the flux rope propagating speed.

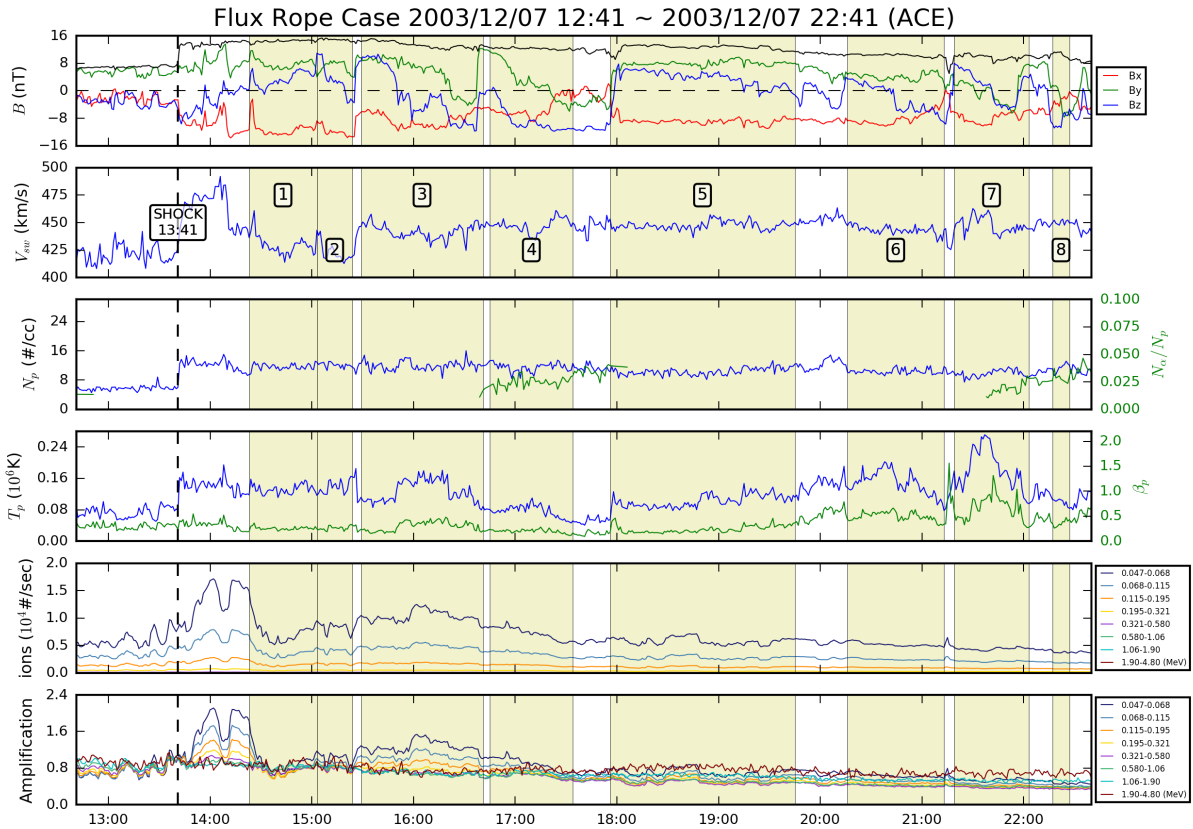


Figure 12. Time series data (ACE) from Dec. 7, 2003, 12:41 UT to Dec. 7, 2003, 22:41 UT. The format is the same as Figure 5.

Figure 14 shows that ACE and Wind are aligned along X_{GSE} axis on the two sides of the Earth. The GSE coordinate of ACE is $(X, Y, Z) = (1.54422 \times 10^6, 2.68164 \times 10^4, 2.28218 \times 10^4)$ km, and the GSE coordinate of Wind is $(X, Y, Z) = (-1.4851 \times 10^6, -1.3105 \times 10^5, -1.1180 \times 10^5)$ km. The separation of ACE and Wind in X_{GSE} direction is 3.02932×10^6 km. The second panels of Figure 12 and Figure 13 show that the average solar wind speed during the interval of flux rope No.3 in Figure 12 and flux rope No.5 in Figure 13 is about 440 km/s. So the propagating time for the flux rope from ACE to Wind is about 115 minutes. The center time of flux rope No.3 in Figure 12 is 16:05 UT, and the center time of flux rope No.5 in Figure 13 is 17:43 UT. The center time shift is 98 minutes, which is close to the estimated propagating time, 115 minutes. Now we confirm that the flux rope No.3 from ACE corresponds to the flux rope No.5 from Wind.

Figure 15 (a) is the reconstructed cross section of flux rope No.3 in Figure 12. Its core B_z field is about 13.5 nT, which is very strong for a small-scale flux rope. The field configuration indicates that this flux rope has right-handed chirality. This flux rope is distorted along x direction. It looks like the remains of two merged flux ropes. Figure 16 (a) is the reconstructed cross section of flux rope No.5 in Figure 13. The core B_z field of flux rope No.5 is about 10 nT, which is relatively weaker compared with its earlier phase. Flux rope No.5 also has right-handed chirality. This is a necessary condition to assure the correspondence between flux rope No.3 from ACE and flux rope No.5 from Wind. Figure 16 (a) shows a flux rope

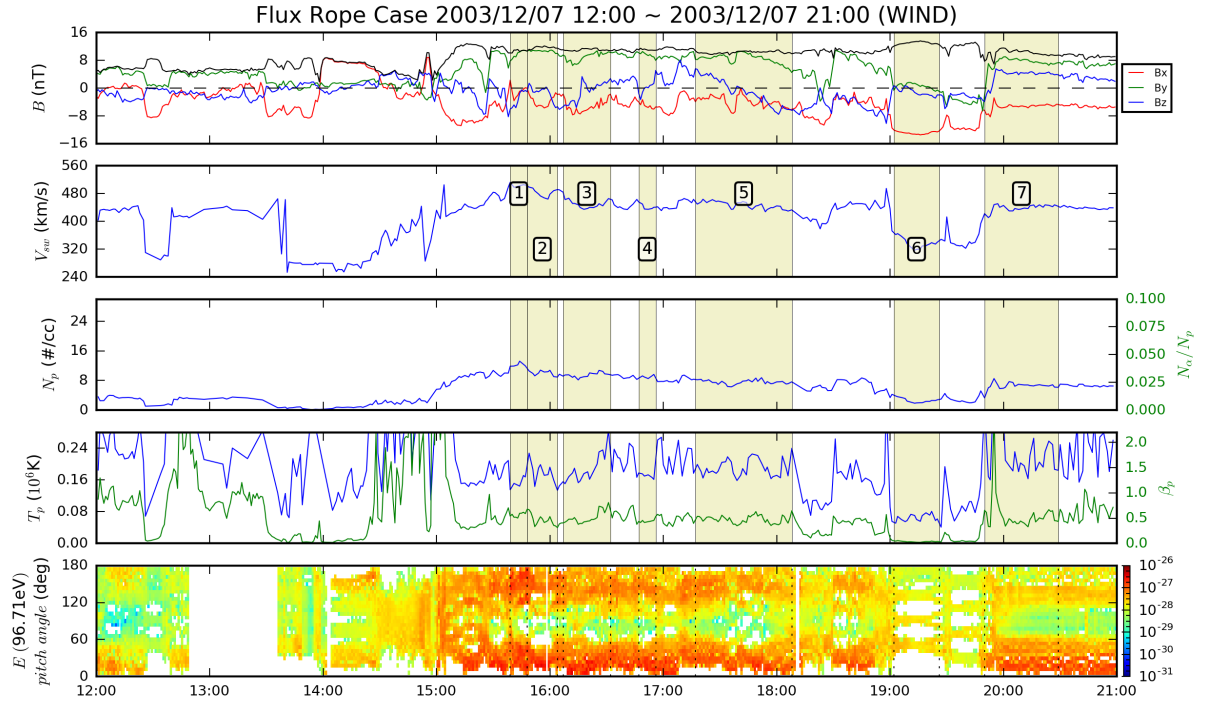


Figure 13. Time series data (Wind) from Dec. 7, 2003, 12:00 UT to Dec. 7, 2003, 21:00 UT. The format is the same as Figure 6.

pinched in the center. This feature can be considered to be evolved from the distorted feature in Figure 15 (a). By checking the axial orientations of flux rope No.3 and flux rope No.5, we found that the angle between them is 45° , indicating the axial orientation change as evolution. The scale sizes of these two flux ropes are similar, which are about 8×10^{-3} AU, i.e., 188 Earth radii. The overall B_z field of flux rope No.5 is lower than that of No.3, which is a reasonable phenomenon in plasma relaxation process. From Figure 15 (a) to Figure 16 (a), we can see a flux rope undergoing the end phase of a merging process, in which its chirality and scale size were kept, but the axial orientation changed by 45° and the overall magnetic field decreased.

The 5th panel in Figure 13 shows that the strong counterstreaming suprathermal electron flux appeared during the interval of flux rope No.5. The counterstreaming suprathermal electrons did not show up in the last case studies (see the 5th panel of Figure 6, in the interval of flux rope No.7). Also we note that the average proton β of flux rope No.3 in Figure 12 and flux rope No.5 in Figure 13 is about 0.5, whereas, in the last case study, this value is higher than 1.0. The strong counterstreaming suprathermal electron flux and low proton β suggest that flux rope No.3 and No.5 may originate from the Sun, instead of being formed in the solar wind. The ions flux within flux rope interval in this case is much stronger than that in the last case (See the 5th panel of Figure 5 and the 5th panel of Figure 12).

4. Conclusions and Discussion

In this paper, we present the preliminary statistical results from our newly-built small-scale flux rope database. The results showed that the occurrence rate of small-scale flux ropes has strong solar cycle dependency. These flux ropes are more likely to appear in slow solar wind streams

2003-12-07 16:00 UT (ACE) 2003-12-07 16:00 UT (WIND)

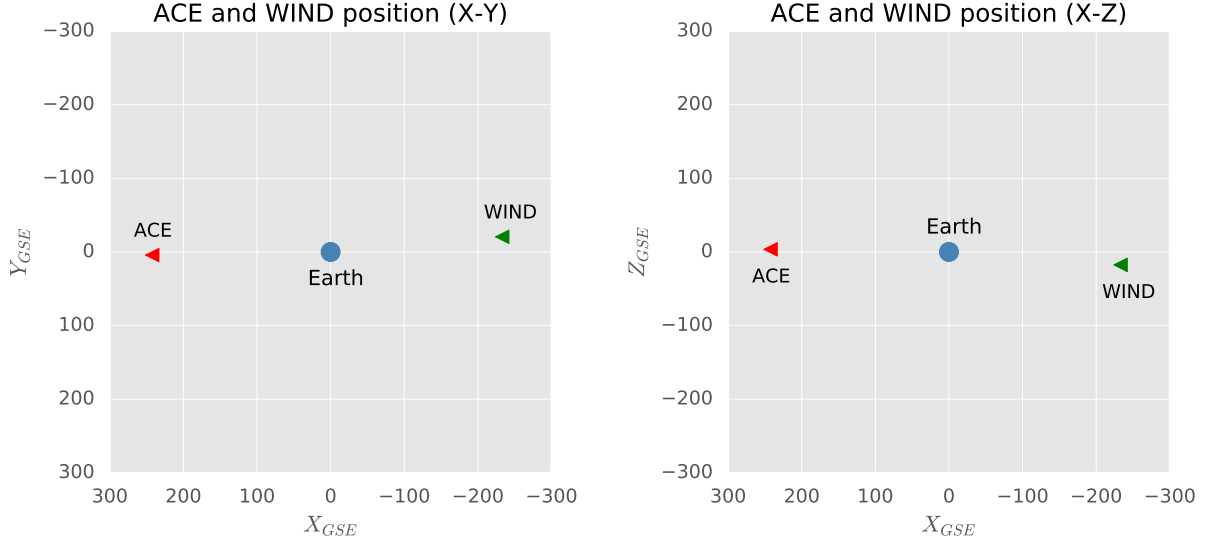
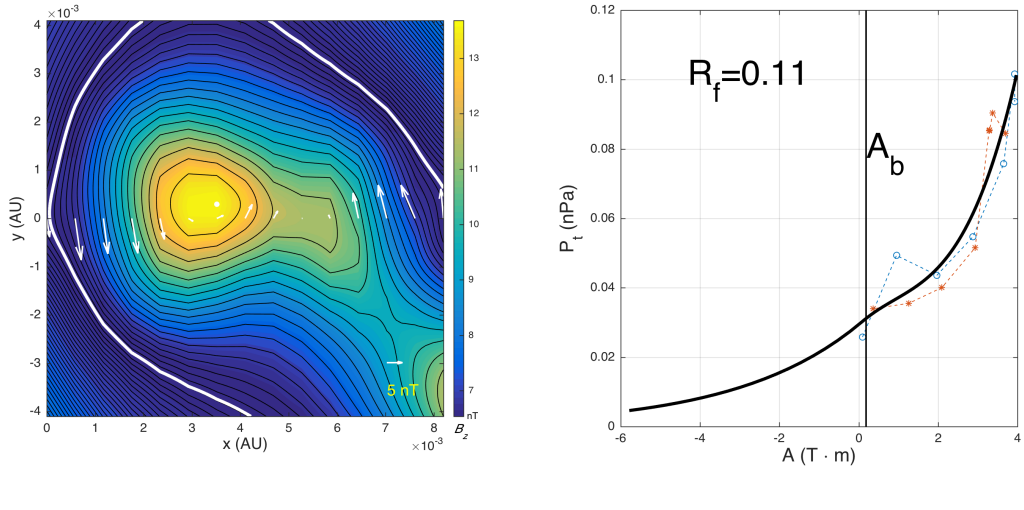


Figure 14. The position of ACE and Wind spacecraft in GSE coordinate. The left panel is the projection on XY-plane, and the right panel is the projection on XZ-plane. Both time stamps of ACE and Wind are July 12th, 2003, 16:00 UT. The unit of all axes is Earth radius.



(a) $\hat{\mathbf{z}} = [-0.8586, 0.4957, -0.1305]$

(b)

Figure 15. GS reconstruction result for flux rope record No.3 (2003 Dec. 7, 15:29 - 16:41 UT). The format is the same as Figure 8.

(speeds about 400 km/s), and possess relatively modest to hight plasma β (distribution peaks around 1). Most of the small-scale flux ropes lay on ecliptic plane with the axial directions along parker spirals.

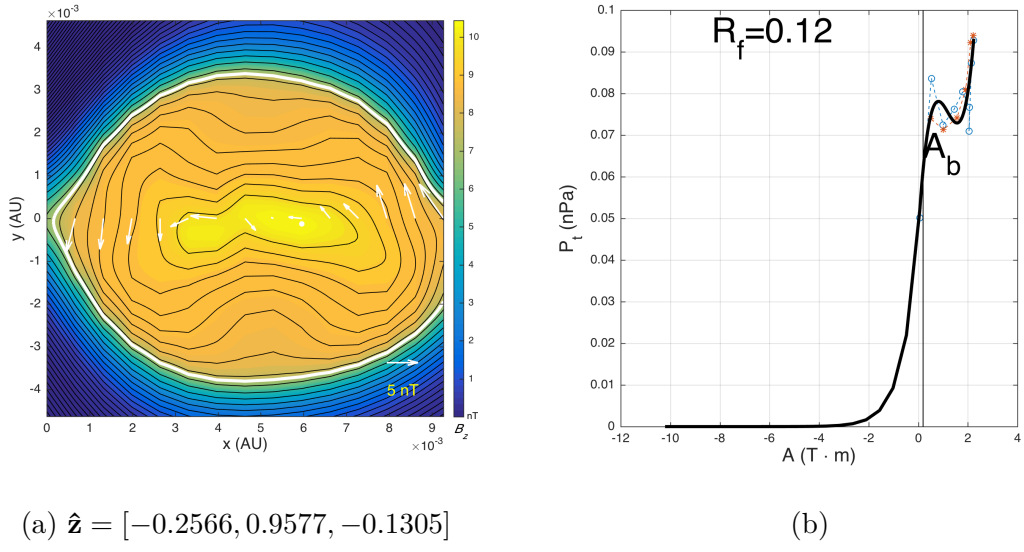


Figure 16. GS reconstruction result for flux rope record No.5 (2003 Dec. 7, 17:18 - 18:08 UT) in Figure 13. The format is the same as Figure 8.

With the combined observation of ACE and Wind spacecraft, we analyzed the temporal evolution of flux ropes and the effect to particle energization. Two case studies are presented, in which the flux rope merging process and the particle energization were observed. In the first case study, we see that a twin flux rope structure was observed by ACE which then became one single flux rope when it was observed by Wind 58 minutes later. In the second case study, we showed the end phase of a flux rope merging process. In both cases, the energetic ions flux was enhanced during the flux rope merging process. These two cases suggest that the flux rope dynamics may play an important role in local particle energization.

Acknowledgments

We would like to thank NASA's Space Physics Data Facility for the Wind and ACE spacecraft data, and University of Helsinki for the Heliospheric Shock Database. We acknowledge NASA grants NNX12AH50G, NNX14AF41G, and NRL contract N00173-14-1-G006 (NNH13ZDA001N) for support. We acknowledge useful discussion with and initial suggestion by Dr. Pete Riley and colleagues on the automated detection of flux ropes by the GS method.

References

- [1] Burlaga L F 1995 *Interplanetary magnetohydrodynamics*, by L. F. Burlaga. *International Series in Astronomy and Astrophysics*, Vol. 3, Oxford University Press. 1995. 272 pages; ISBN13: 978-0-19-508472-6 **3**
- [2] Moldwin M B, Ford S, Lepping R, Slavin J and Szabo A 2000 *Journal of Geophysical Research: Space Physics* **27** 57–60
- [3] Cartwright M L and Moldwin M B 2010 *Journal of Geophysical Research (Space Physics)* **115** A08102
- [4] Feng H Q, Wu D J, Lin C C, Chao J K, Lee L C and Lyu L H 2008 *Journal of Geophysical Research (Space Physics)* **113** A12105
- [5] Hu Q and Sonnerup B U Ö 2001 *Geophysical Research Letters* **28** 467–470
- [6] Yu W, Farrugia C J, Lugaz N, Galvin A B, Kilpua E K, Kucharek H, Moestl C, Leitner M, Torbert R B, Simunac K, Luhmann J G, Szabo A, Ogilvie K W and Sauvaud J 2013 *AGU Fall Meeting Abstracts*
- [7] Borovsky J E 2008 *Journal of Geophysical Research (Space Physics)* **113** A08110

- [8] Zheng J and Hu Q 2016 *15th AIAC/The Science of Ed Stone: Celebrating his 80th Birthday* IOP Conf. Series ed Zank G P
- [9] Khabarova O V, Zank G P, Li G, Malandraki O E, le Roux J A and Webb G M 2016 *The Astrophysical Journal* **827** 122 URL <http://stacks.iop.org/0004-637X/827/i=2/a=122>
- [10] le Roux J A, Zank G P, Webb G M and Khabarova O V 2016 *The Astrophysical Journal* **827** 47 URL <http://stacks.iop.org/0004-637X/827/i=1/a=47>
- [11] Matsumoto Y, Amano T, Kato T N and Hoshino M 2015 *Science* **347** 974–978
- [12] Khabarova O, Zank G P, Li G, le Roux J A, Webb G M, Dosch A and Malandraki O E 2015 *The Astrophysical Journal* **808** 181 (Preprint 1504.06616)
- [13] Karimabadi H, Roytershteyn V, Vu H X, Omelchenko Y A, Scudder J, Daughton W, Dimmock A, Nykyri K, Wan M, Sibeck D, Tatineni M, Majumdar A, Loring B and Geveci B 2014 *Physics of Plasmas* **21** 062308
- [14] Trenchi L, Bruno R, Telloni D, D'amicis R, Marcucci M F, Zurbuchen T H and Weberg M 2013 *The Astrophysical Journal* **770** 11
- [15] Tassein J A, Matthaeus W H, Wan M, Osman K T, Ruffolo D and Giacalone J 2013 *The Astrophysical Journal* **776** L8
- [16] Retinò A, Sundkvist D, Vaivads A, Mozer F, André M and Owen C J 2007 *Nature Physics* **3** 236–238
- [17] Chen L J, Bhattacharjee A, Puhl-Quinn P A, Yang H, Bessho N, Imada S, Mühlbacher S, Daly P W, Lefebvre B, Khotyaintsev Y, Vaivads A, Fazakerley A and Georgescu E 2008 *Nature Physics* **4** 19–23
- [18] Drake J F, Swisdak M, Che H and Shay M A 2006 *Nature* **443** 553–556
- [19] Zank G P, Adhikari L, Hunana P, Shiota D, Bruno R and Telloni D 2017 *The Astrophysical Journal* **835** 147 URL <http://stacks.iop.org/0004-637X/835/i=2/a=147>
- [20] Tassein J A, Ruffolo D, Matthaeus W H and Wan M 2016 *Geophysical Research Letters* **43** 3620–3627
- [21] Tassein J A, Ruffolo D, Matthaeus W H, Wan M, Giacalone J and Neugebauer M 2015 *The Astrophysical Journal* **812** 68
- [22] Neugebauer M and Giacalone J 2015 *Journal of Geophysical Research (Space Physics)* **120** 8281–8287
- [23] Osman K T, Matthaeus W H, Gosling J T, Greco A, Servidio S, Hnat B, Chapman S C and Phan T D 2014 *Physical Review Letters* **112** 215002 (Preprint 1403.4590)
- [24] Karimabadi H, Roytershteyn V, Wan M, Matthaeus W H, Daughton W, Wu P, Shay M, Loring B, Borovsky J, Leonardis E, Chapman S C and Nakamura T K M 2013 *Physics of Plasmas* **20** 012303
- [25] Greco A, Matthaeus W H, Servidio S, Chuaychai P and Dmitruk P 2009 *The Astrophysical Journal* **691** L111–L114
- [26] le Roux J A, Zank G P, Webb G M and Khabarova O 2015 *The Astrophysical Journal* **801** 112 URL <http://stacks.iop.org/0004-637X/801/i=2/a=112>
- [27] Zank G P, Hunana P, Mostafavi P, Le Roux J A, Li G, Webb G M, Khabarova O, Cummings A, Stone E and Decker R 2015 *The Astrophysical Journal* **814** 137
- [28] Zank G P, le Roux J A, Webb G M, Dosch A and Khabarova O 2014 *The Astrophysical Journal* **797** 28 URL <http://stacks.iop.org/0004-637X/797/i=1/a=28>
- [29] Hu Q and Sonnerup B U O 2002 *Journal of Geophysical Research: Space Physics* **107** SSH 10–1–SSH 10–15 ISSN 2156-2202 URL <http://dx.doi.org/10.1029/2001JA000293>
- [30] Hu Q, Smith C W, Ness N F and Skoug R M 2003 *Geophysical Research Letters* **30** 1385
- [31] Hu Q, Smith C W, Ness N F and Skoug R M 2005 *Journal of Geophysical Research (Space Physics)* **110** A09S03
- [32] Hu Q, Farrugia C J, Osherovich V A, Möstl C, Szabo A, Ogilvie K W and Lepping R P 2013 *Solar Physics* **284** 275–291
- [33] Hu Q, Qiu J, Dasgupta B, Khare A and Webb G M 2014 *The Astrophysical Journal* **793** 53 (Preprint 1408.1470)
- [34] Hu Q, Qiu J and Krucker S 2015 *Journal of Geophysical Research: Space Physics* **120** 1
- [35] Hu Q 2016 *International Solar Wind 14 Conference (AIP Conf. Series* vol 1720) ed Wang L, Bruno R, Möbius E, Vourlidas A and Zank G p 040005
- [36] Hu Q 2016 *Solar Physics* Submitted
- [37] Khabarova O V, Zank G P, Malandraki O E, Li G, le Roux J A and Webb G M 2017 *Sun and Geosphere* **12** 23–30
- [38] Linton M G 2006 *Journal of Geophysical Research: Space Physics* **111** n/a–n/a ISSN 2156-2202 a12S09 URL <http://dx.doi.org/10.1029/2006JA011891>